CSIT-Driven Spectral Precoding for Sidelobe Suppression in Multicarrier Modulation

Vahid Vahidpour, Roberto López-Valcarce
atlanTTic, Universidade de Vigo, Spain
{vahidpour,valcarce}@gts.uvigo.es

Josep Sala-Álvarez
Universitat Politècnica de Catalunya, Spain
josep.sala@upc.edu

***Abstract*—We propose a channel-aware spectral precoding scheme for multicarrier modulation with channel state information at the transmitter (CSIT) that minimizes out-of-band radiation (OBR) under transmit power and mutual information constraints. The precoder is obtained by solving a constrained optimization problem via a fixed-point algorithm that incorporates reverse waterfilling and spectral shaping through a semi-unitary front-end. The spectral invariance under unitary rotations is leveraged to embed CSIT without altering the transmit power spectral density. This enables low-complexity receiver designs based on zero-forcing (ZF) or successive interference cancellation (SIC) strategies. Numerical results over block-fading multipath channels show that the proposed design achieves better OBR reduction and improved symbol error rates compared to existing schemes such as pre-equalized and spectrally precoded OFDM (PSP-OFDM) and null-subcarrier precoding. The SIC receiver achieves the best performance in the medium-to-high SNR regime, confirming the effectiveness of the proposed framework.**

***Index Terms*—Multicarrier modulation, spectral precoding, sidelobe suppression, channel state information at transmitter, successive interference cancellation.**

I. Introduction

Multicarrier modulation has become a central component of modern wireless systems due to its robustness against frequency-selective fading, spectral flexibility, and compatibility with MIMO techniques. Among them, orthogonal frequency-division multiplexing (OFDM) remains the most widely adopted. However, the abrupt transitions induced by rectangular pulse shaping yield power spectral density (PSD) sidelobes that decay slowly as f^{-2}, causing considerable out-of-band radiation (OBR) and interference to adjacent channels [1], [2]. The conventional approach to reduce OBR, i.e., nulling edge subcarriers, comes at the cost of reduced spectral efficiency due to persistent leakage from remaining tones.

Several techniques have been proposed to address this issue. Time-domain methods, including waveform shaping [3], [4], filtering [5]–[7], windowing [8]–[10], and time-domain suppression alignment [11], [12]. Alternatively, frequency-domain methods modify the transmitted symbols prior to the inverse fast Fourier transform (IFFT). These include nonlinear mapping [13], cancellation carriers insertion [14], [15], and linear spectral precoding [16]–[22], which has emerged as an attractive solution due to its analytical tractability and compatibility with standard OFDM processing chains.

Linear precoding strategies can be broadly categorized into three classes: spectral nulling, N-continuous precoding, and band-specific power minimization (BSPM). The BSPM approach is particularly appealing as it formulates spectral shaping as a quadratic program targeting leakage in specific frequency regions. Beyond spectral control, precoding naturally introduces frequency diversity, which improves reliability over fading channels at the expense of higher receiver complexity [19], [23], [24]. Recent works have also explored incorporating channel-state information at the transmitter (CSIT) into the design. The PSP-OFDM scheme in [25] pre-equalizes the channel via a cascaded design, combining (N-continuous) spectral shaping, waterfilling-based power allocation, and a unitary rotation for Peak to Average Power Ratio (PAPR) reduction, while applying linear minimum mean squared error (LMMSE) decoding at the receiver.

In this work, we revisit BSPM-based spectral precoding from a constrained optimization perspective and propose a CSIT-aware framework that jointly minimizes OBR while satisfying power and mutual information (MI) constraints. The optimal precoder structure is derived via first-order conditions and obtained through an efficient fixed-point iteration that incorporates reverse waterfilling and semi-unitary shaping. Under CSIT, we exploit the spectral invariance under unitary rotations to tailor the effective channel for receiver-side decoding without altering the transmit PSD. This leads to two decoding strategies: a ZF receiver based on SVD diagonalization, and an SIC receiver based on geometric mean decomposition (GMD), which provides equalized post-processing noise variance and stronger diversity. Simulations over block-fading multipath channels demonstrate substantially improved spectral confinement and mid/high-SNR error rate compared to both PSP-OFDM and null-subcarrier baselines.

Notation: a, A denote scalars; $\mathbf{a}$, $\mathbf{A}$ resp. denote vectors and matrices. Transpose and conjugate transpose are written $\mathbf{A}^{\mathsf{T}}$ and $\mathbf{A}^{\mathsf{H}}$. $\mathsf{Tr}(\mathbf{A})$, $|\mathbf{A}|$ are the trace and determinant of $\mathbf{A}$. The $N \times N$ identity is $\mathbf{I}_N$, and $\mathbf{0}$ denotes an all-zeros matrix of proper size. Statistical expectation is $\mathsf{E}[\cdot]$; $\mathsf{Diag}\{\cdot\}$ places its arguments on the main diagonal of a square matrix. The hard slicer $\mathsf{DEC}_{\mathbb{A}}\{\cdot\}$ returns componentwise the closest element of $\mathbb{A} \subset \mathbb{C}$.

Supported by MICIU/AEI/10.13039/501100011033 and by ERDF/EU under grants PID2022-136512OB-C21 and PID2022-136512OB-C22.

II. System Model

We consider a multicarrier OFDM transmitter in which an N-point IFFT sets the subcarrier grid, and a guard of l_g samples extends each block to $L \triangleq N + l_g$. Let the set of active tones be $\mathcal{K} = \{k_1, \ldots, k_K\}$ with $|\mathcal{K}| = K \leq N$. Given $D \leq K$, the m-th block data vector $\mathbf{d}_m = [d_1^{(m)}, \ldots, d_D^{(m)}]^{\mathsf{T}} \in \mathbb{A}^D$ is expanded by a memoryless linear map $\mathbf{G} \in \mathbb{C}^{K \times D}$ onto the K active tones:

$$\mathbf{x}_m = \mathbf{G}\mathbf{d}_m \in \mathbb{C}^K, \tag{1}$$

where $\eta \triangleq D/K \leq 1$ and $R \triangleq K - D \geq 0$ quantify, resp., coding rate and redundancy. Let $x_k^{(m)}$ be the component of $\mathbf{x}_m$ tied to $k \in \mathcal{K}$. Given a shaping pulse $h_{\mathrm{P}}[n]$ with DTFT $H_{\mathrm{P}}(\mathrm{e}^{\jmath\omega})$, the discrete-time baseband sequence is

$$s[n] = \sum_{m=-\infty}^{\infty} \sum_{k \in \mathcal{K}} x_k^{(m)}\, h_{\mathrm{P}}[n - mL]\, \mathrm{e}^{\jmath \frac{2\pi}{N} k(n-mL)}. \tag{2}$$

For cyclic prefix (CP) OFDM, $h_{\mathrm{P}}[n] = 1$ for $0 \leq n < L$ and 0 otherwise; zero-padded (ZP) and other guards follow by modifying $h_{\mathrm{P}}[n]$ accordingly [26]. Let T_s be the sampling interval, and $\Delta_f = 1/(NT_s)$ the subcarrier spacing. The continuous-time baseband signal is

$$s(t) = \sum_{n=-\infty}^{\infty} s[n]\, h_{\mathrm{I}}(t - nT_s), \tag{3}$$

where $h_{\mathrm{I}}(t)$ is the impulse response of the interpolation filter in the Digital-to-Analog Converter, with frequency response $H_{\mathrm{I}}(f)$. We assume $\mathbf{d}_m \in \mathbb{A}^D$ is zero-mean and temporally white across OFDM blocks, i.e., $\mathsf{E}\big[\mathbf{d}_m \mathbf{d}_{m-\ell}^{\mathsf{H}}\big] = \delta[\ell]\mathbf{I}_D$. For the k-th active tone, define $a_k(f) \triangleq H_{\mathrm{P}}^*(\mathrm{e}^{\jmath 2\pi (f - k\Delta_f)T_s})$ and collect $\mathbf{a}(f) \triangleq [a_{k_1}(f), \ldots, a_{k_K}(f)]^{\mathsf{T}} \in \mathbb{C}^K$. Then by [26, Th. 1], the continuous-time waveform $s(t)$ in (3) is wide-sense cyclostationary with period LT_s. Its (cycle-averaged) PSD is

$$P_s(f) = \frac{|H_{\mathrm{I}}(f)|^2}{LT_s} \mathbf{a}^{\mathsf{H}}(f) \mathbf{G}\mathbf{G}^{\mathsf{H}}\, \mathbf{a}(f). \tag{4}$$

At the receiver side, we assume perfect CSIT and standard CP-OFDM conditions (channel support within the CP length, and block-constant over one OFDM symbol). Then, after CP removal and N-point FFT, the frequency-domain channel over $\mathcal{K}$ is diagonal:

$$\mathbf{H} \triangleq \mathsf{Diag}\left\{H_c[k_1], \ldots, H_c[k_K]\right\} \in \mathbb{C}^{K \times K}, \tag{5}$$

where $H_c[k]$ denotes the N-point DFT sample of the channel impulse response at bin k. Dropping the symbol index in (1) and writing $\mathbf{x} = \mathbf{G}\mathbf{d}$, and with ideal time/frequency synchronization, the received vector $\mathbf{r} \in \mathbb{C}^K$ is

$$\mathbf{r} = \mathbf{H}\mathbf{x} + \mathbf{n} = \mathbf{H}\mathbf{G}\mathbf{d} + \mathbf{n}, \tag{6}$$

where the noise $\mathbf{n} \in \mathbb{C}^K$ is circularly symmetric complex Gaussian with zero mean and covariance $\mathsf{E}\big[\mathbf{n}\mathbf{n}^{\mathsf{H}}\big] = \sigma^2 \mathbf{I}_K$. When CSIT is available, $\mathbf{G}$ may be chosen as a (possibly channel-dependent) linear precoder satisfying design constraints (e.g., spectral shaping via $\mathbf{G}\mathbf{G}^{\mathsf{H}}$ in (4)) while the detector accounts for $\mathbf{H}\mathbf{G}$ in (6).

III. Problem Statement

The spectral precoder $\mathbf{G}$ must jointly address (i) spectral confinement, (ii) transmit-power efficiency, and (iii) end-to-end reliability. We quantify these aspects as follows.

1) Out-of-band radiation (OBR): Following a BSPM approach, given a spectral weight $W(f) \geq 0$ supported on a prescribed region $\mathcal{B}$, the weighted radiated power is

$$P_W \triangleq \int_{-\infty}^{\infty} W(f) P_s(f) \mathrm{d}f = \mathsf{Tr}\big(\mathbf{G}^{\mathsf{H}} \mathbf{A} \mathbf{G}\big), \tag{7}$$

where the matrix $\mathbf{A} \in \mathbb{C}^{K \times K}$ is given by

$$\mathbf{A} \triangleq \frac{1}{LT_s} \int_{-\infty}^{\infty} W(f)\, |H_{\mathrm{I}}(f)|^2 \mathbf{a}(f) \mathbf{a}^{\mathsf{H}}(f) \mathrm{d}f, \tag{8}$$

and is Hermitian positive semidefinite by construction. The choice of $W(f)$ specifies how different frequency components contribute to the total OBR. Uniform leakage control over $\mathcal{B}$ is achieved by setting $W(f) = 1$ for $f \in \mathcal{B}$ and $W(f) = 0$ elsewhere; nonuniform $W(f)$ allows prioritizing specific subbands.

2) Transmit Power: Under the stated assumptions on data vector $\mathbf{d}$, the average power of the precoded vector $\mathbf{x}$ is

$$\mathsf{E}\big[\|\mathbf{x}\|^2\big] = \mathsf{Tr}\big(\mathbf{G}^{\mathsf{H}}\mathbf{G}\big). \tag{9}$$

3) Mutual information (MI): Assuming Gaussian signaling and perfect CSIT, the MI between the transmitted data and the received vector in (6) is

$$\begin{aligned} \mathcal{I}(\mathbf{d}; \mathbf{r}) &= \log \left| \mathbf{I}_K + \frac{1}{\sigma^2} \mathbf{H}\mathbf{G}\mathbf{G}^{\mathsf{H}}\mathbf{H}^{\mathsf{H}} \right| \\ &= \log \left| \mathbf{I}_D + \mathbf{G}^{\mathsf{H}}\mathbf{C}\mathbf{G} \right|, \end{aligned} \tag{10}$$

where $\mathbf{C} \triangleq \frac{1}{\sigma^2}\mathbf{H}^{\mathsf{H}}\mathbf{H}$ is the (scaled) channel covariance matrix.

We aim to design $\mathbf{G}$ so as to minimize the OBR, subject to a transmit power budget and an MI target requirement. Formally, the problem is posed as:

$$\min_{\mathbf{G}} \ \mathsf{Tr}\big(\mathbf{G}^{\mathsf{H}}\mathbf{A}\mathbf{G}\big) \quad \text{s. to} \begin{cases} \mathsf{Tr}\big(\mathbf{G}^{\mathsf{H}}\mathbf{G}\big) \leq P_{\max}, & \text{(11a)} \\ \log \left| \mathbf{I}_D + \mathbf{G}^{\mathsf{H}}\mathbf{C}\mathbf{G} \right| \geq \mathcal{I}_{\min}, & \text{(11b)} \end{cases}$$

with $P_{\max} > 0$ and $\mathcal{I}_{\min} > 0$ prescribed. Note that, if $\mathbf{G}_\star$ is any optimizer of (11), then the MI constraint (11b) must be tight. Indeed, if $\mathbf{G}_\star$ satisfied (11b) with strict inequality, then the scaled precoder $(1 - \epsilon)\mathbf{G}_\star$ for sufficiently small $\epsilon > 0$ would remain feasible and yield a strictly lower objective value, contradicting the optimality of $\mathbf{G}_\star$. On the other hand, it is not evident whether the power constraint (11a) is tight at the optimum or not.

Problem (11) is not convex. After analyzing feasibility and expressing a first-order optimality condition, we shall propose an iterative approach to find a suitable solution.

A. Feasibility

Feasibility of problem (11) depends on the pair $(P_{\max}, \mathcal{I}_{\min})$. It can be assessed through either of the following approaches:

1) Fixing the power budget: Suppose $P_{\max}$ is given. Consider the auxiliary problem:

$$\mathcal{I}_0 \triangleq \max_{\mathbf{G}} \log\left|\mathbf{I}_D + \mathbf{G}^{\mathsf{H}}\mathbf{C}\mathbf{G}\right| \text{ s. to } \mathsf{Tr}\big(\mathbf{G}^{\mathsf{H}}\mathbf{G}\big) \le P_{\max}. \quad (12)$$

This is a standard waterfilling problem [27] whose solution satisfies the power constraint (11a) with equality. Problem (11) is feasible if and only if $\mathcal{I}_{\min} \le \mathcal{I}_0$; otherwise, the power budget $P_{\max}$ is insufficient to meet the MI requirement $\mathcal{I}_{\min}$. Note that $\mathcal{I}_0$ is a function of $P_{\max}$.

2) Fixing the MI requirement: Suppose $\mathcal{I}_{\min}$ is fixed. Consider the dual auxiliary problem:

$$P_0 \triangleq \min_{\mathbf{G}} \mathsf{Tr}\big(\mathbf{G}^{\mathsf{H}}\mathbf{G}\big) \text{ s. to } \log\left|\mathbf{I}_D + \mathbf{G}^{\mathsf{H}}\mathbf{C}\mathbf{G}\right| \ge \mathcal{I}_{\min}. \quad (13)$$

Note that at the solution of (13) the constraint must be tight. Then (11) is feasible if and only if $P_{\max} \ge P_0$. The threshold P_0 depends on $\mathcal{I}_{\min}$. Problem (13), whose solution is given in Appendix A, constitutes a *reversed* formulation of the standard waterfilling problem: MI is imposed as a constraint and the transmit power is minimized.

B. First-order Condition

Assume (11) is feasible. The Lagrangian is given by

$$\mathcal{L} = \mathsf{Tr}\big(\mathbf{G}^{\mathsf{H}}\mathbf{A}\mathbf{G}\big) + \mu\big(\mathsf{Tr}\big(\mathbf{G}^{\mathsf{H}}\mathbf{G}\big) - P_{\max}\big) + \alpha\big(\mathcal{I}_{\min} - \log\big|\mathbf{I}_D + \mathbf{G}^{\mathsf{H}}\mathbf{C}\mathbf{G}\big|\big), \quad (14)$$

with Lagrange multipliers $\mu \ge 0$, $\alpha \ge 0$ associated with the power and MI constraints, respectively. Recall now the matrix derivative [28]:

$$\frac{\mathrm{d}}{\mathrm{d}\mathbf{X}} \log\left|\delta\mathbf{I} + \mathbf{X}^{\mathsf{H}}\mathbf{M}\mathbf{X}\right| = \mathbf{M}\mathbf{X}\left(\delta\mathbf{I} + \mathbf{X}^{\mathsf{H}}\mathbf{M}\mathbf{X}\right)^{-1}, \quad (15)$$

for any $\delta > 0$ and Hermitian martix $\mathbf{M}$. Applying this to (14), the gradient of $\mathcal{L}$ with respect to $\mathbf{G}$ is

$$\frac{\mathrm{d}\mathcal{L}}{\mathrm{d}\mathbf{G}} = \mathbf{A}\mathbf{G} + \mu\mathbf{G} - \alpha\mathbf{C}\mathbf{G}\left(\mathbf{I}_D + \mathbf{G}^{\mathsf{H}}\mathbf{C}\mathbf{G}\right)^{-1}. \quad (16)$$

At any stationary point this derivative must vanish. Thus, $\mathbf{G}$ satisfies the first-order condition:

$$(\mathbf{A} + \mu\,\mathbf{I}_K)\,\mathbf{G} = \alpha\mathbf{C}\mathbf{G}\left(\mathbf{I}_D + \mathbf{G}^{\mathsf{H}}\mathbf{C}\mathbf{G}\right)^{-1}, \quad (17)$$

for some multipliers $\mu \ge 0$, $\alpha \ge 0$ to be determined.

IV. Proposed Precoder

We propose an iterative method to solve the stationarity condition (17). Let the power multiplier $\mu \ge 0$ be fixed. We aim to find a pair $(\mathbf{G}, \alpha)$ satisfying (17) such that the MI constraint is met with equality. The resulting transmit power $\mathsf{Tr}\big(\mathbf{G}^{\mathsf{H}}\mathbf{G}\big)$ depends on the chosen μ, and may or may not satisfy the power constraint. We state the following conjecture:

Conjecture 1: Assume Problem (11) is feasible. For each $\mu \ge 0$, let the pair $(\mathbf{G}_\mu, \alpha_\mu)$ be such that

$$(\mathbf{A} + \mu\,\mathbf{I}_K)\,\mathbf{G}_\mu = \alpha_\mu\mathbf{C}\mathbf{G}_\mu\left(\mathbf{I}_D + \mathbf{G}_\mu^{\mathsf{H}}\mathbf{C}\mathbf{G}_\mu\right)^{-1}, \quad (18)$$

$$\log|\mathbf{I}_D + \mathbf{G}_\mu^{\mathsf{H}}\mathbf{C}\mathbf{G}_\mu| = \mathcal{I}_{\min}. \quad (19)$$

Then:

Algorithm 1: Iterative search for BSPM precoder

Input: Initial $\mathbf{G}_0$, $\mu_0 > 0$

for $i = 1, 2, \ldots$ *until convergence* **do**

$\widetilde{\mathbf{G}}_i \leftarrow \big(\mathbf{A} + \mu_{i-1}\mathbf{I}_K\big)^{-1}\mathbf{C}\mathbf{G}_{i-1}\big(\mathbf{I}_D + \mathbf{G}_{i-1}^{\mathsf{H}}\mathbf{C}\mathbf{G}_{i-1}\big)^{-1}$

Use bisection to find $\alpha_i \ge 0$ such that

$$\log\left|\mathbf{I}_D + \alpha_i^2\,\widetilde{\mathbf{G}}_i^{\mathsf{H}}\mathbf{C}\,\widetilde{\mathbf{G}}_i\right| = \mathcal{I}_{\min}$$

$\mathbf{G}_i \leftarrow \alpha_i\widetilde{\mathbf{G}}_i$

$\mu_i \leftarrow \mu_{i-1} \cdot \dfrac{\mathsf{Tr}\big(\mathbf{G}_i^{\mathsf{H}}\mathbf{G}_i\big)}{P_{\max}}$

end

- The power $\mathsf{Tr}\big(\mathbf{G}_\mu^{\mathsf{H}}\mathbf{G}_\mu\big)$ is monotonically decreasing in μ;
- The OBR $\mathsf{Tr}\big(\mathbf{G}_\mu^{\mathsf{H}}\mathbf{A}\mathbf{G}_\mu\big)$ is monotonically increasing in μ.

If Conjecture 1 is true, then the optimal solution to (11) corresponds to the value of μ such that $\mathsf{Tr}\big(\mathbf{G}_\mu^{\mathsf{H}}\mathbf{G}_\mu\big) = P_{\max}$, or to $\mu = 0$ if this already yields power below $P_{\max}$.

To compute $(\mathbf{G}_\mu, \alpha_\mu)$ for a given μ, let $\hat{\mathbf{G}}_0$ be an initial estimate; then for $i = 1, 2, \ldots$, repeat until convergence:

- **Step 1:** Update

$$\widetilde{\mathbf{G}}_i = \big(\mathbf{A}+\mu\mathbf{I}_K\big)^{-1}\mathbf{C}\hat{\mathbf{G}}_{i-1}\big(\mathbf{I}_D+\hat{\mathbf{G}}_{i-1}^{\mathsf{H}}\mathbf{C}\hat{\mathbf{G}}_{i-1}\big)^{-1} \quad (20)$$

- **Step 2:** Find $\hat{\alpha}_i \ge 0$ such that

$$\log\left|\mathbf{I}_D + \hat{\alpha}_i^2\widetilde{\mathbf{G}}_i^{\mathsf{H}}\mathbf{C}\widetilde{\mathbf{G}}_i\right| = \mathcal{I}_{\min}. \quad (21)$$

- **Step 3:** Set $\hat{\mathbf{G}}_i = \hat{\alpha}_i\widetilde{\mathbf{G}}_i$.

If this iteration converges, we set $(\mathbf{G}_\mu, \alpha_\mu)$ to the resulting limiting values of $(\hat{\mathbf{G}}_i, \hat{\alpha}_i)$, which will satisfy both (18) and (19). Regarding Step 2, let $\beta_1 \ge \ldots \ge \beta_D \ge 0$ be the ordered eigenvalues of the positive semidefinite matrix $\widetilde{\mathbf{G}}_i^{\mathsf{H}}\mathbf{C}\widetilde{\mathbf{G}}_i$, and define

$$g(a) \triangleq \sum_{\ell=1}^{D} \log(1 + a\,\beta_\ell). \quad (22)$$

Then g is strictly increasing in $a \in [0, \infty)$, with $g(0) = 0$ and $\lim_{a\to\infty} g(a) = \infty$. Thus, $g(a) = \mathcal{I}_{\min}$ admits a unique solution $a_\star > 0$ (which can be found, e.g., via bisection), and we set $\hat{\alpha}_i = \sqrt{a_\star}$.

To solve (11), one may line-search μ to enforce the power constraint with equality. A more efficient alternative embeds the update of μ within the iteration, as in Algorithm 1. Guided by Conjecture 1, increase μ if the power exceeds $P_{\max}$ and decrease it otherwise.

V. Decoder-Aware Precoder Design

Let $\mathbf{G}_\star$ be the precoder returned by Algorithm 1 and set $M \triangleq \mathrm{rank}(\mathbf{G}_\star) \le D$. As in standard waterfilling (12), it may occur that $M < D$, i.e., some weak modes are not used and only M data streams are effectively transmitted. Write the SVD of $\mathbf{G}_\star = \mathbf{U}_\star\mathbf{\Sigma}_\star\mathbf{V}_\star^{\mathsf{H}}$, with $\mathbf{U}_\star \in \mathbb{C}^{K\times M}$ and $\mathbf{V}_\star \in \mathbb{C}^{D\times M}$ semi-unitary, and $\mathbf{\Sigma}_\star \in \mathbb{C}^{M\times M}$ diagonal and nonsingular. We may then redefine the precoder as

$\mathbf{G}_\star = \mathbf{U}_\star \mathbf{\Sigma}_\star \in \mathbb{C}^{K\times M}$, which preserves the objective and both constraints in (11). With this reduction (only needed if $M < D$), the input–output model (6) holds verbatim after the dimension change.

Further, note that for any unitary $\mathbf{V} \in \mathbb{C}^{M\times M}$, the rotated precoder $\mathbf{G}_\star\mathbf{V}$ induces exactly the same PSD (4) and OBR (7). This degree of freedom has been used to optimize auxiliary aspects such as on-line complexity and PAPR without altering the spectrum [25], [29]. Here, under CSIT, we exploit it to tailor the *effective channel* to the chosen decoder.

A. Zero-Forcing decoder with CSIT

Let the SVD of the effective channel $\mathbf{HG}_\star$ be

$$\mathbf{HG}_\star = \mathbf{U}_h \mathbf{\Gamma}_h \mathbf{V}_h^{\mathsf{H}}, \tag{23}$$

where $\mathbf{U}_h \in \mathbb{C}^{K\times M}$ is semi-unitary, $\mathbf{V}_h \in \mathbb{C}^{M\times M}$ is unitary, and $\mathbf{\Gamma}_h = \mathsf{Diag}\{\gamma_1, \ldots, \gamma_M\}$ contains the singular values. We transmit $\mathbf{x} = \mathbf{U}_\star \mathbf{\Sigma}_\star \mathbf{V}_h \mathbf{d}$, yielding the received signal

$$\mathbf{r} = \mathbf{Hx} + \mathbf{n} = \mathbf{U}_h \mathbf{\Gamma}_h \mathbf{d} + \mathbf{n}. \tag{24}$$

A ZF decoder applies $\mathbf{\Gamma}_h^{-1}\mathbf{U}_h^{\mathsf{H}}$ to obtain

$$\mathbf{\Gamma}_h^{-1}\mathbf{U}_h^{\mathsf{H}}\mathbf{r} = \mathbf{d} + \mathbf{w}_h, \tag{25}$$

where $\mathbf{w}_h = \mathbf{\Gamma}_h^{-1}\mathbf{U}_h^{\mathsf{H}}\mathbf{n}$ is zero-mean Gaussian with covariance $\sigma^2\mathbf{\Gamma}_h^{-2}$. A hard decision produces the final estimate, $\hat{\mathbf{d}} = \mathsf{DEC}_{\mathbb{A}}\{\mathbf{\Gamma}_h^{-1}\mathbf{U}_h^{\mathsf{H}}\mathbf{r}\}$. The total post-equalization noise power is $\sigma^2\mathsf{Tr}(\mathbf{\Gamma}_h^{-2})$. As in standard ZF, noise enhancement occurs when some singular values γ_i are small.

B. SIC decoder with CSIT

To obtain a structure amenable to SIC, apply the geometric mean decomposition (GMD) [30] to the effective channel:

$$\mathbf{HG}_\star = \gamma\, \mathbf{Q}_h \mathbf{R}_h \mathbf{P}_h^{\mathsf{H}}, \tag{26}$$

where $\mathbf{Q}_h \in \mathbb{C}^{K\times M}$ is semi-unitary, $\mathbf{P}_h \in \mathbb{C}^{M\times M}$ is unitary, $\mathbf{R}_h \in \mathbb{C}^{M\times M}$ is unit upper triangular (ones on the diagonal), and $\gamma = \big(\prod_{i=1}^{M}\gamma_i\big)^{1/M}$ is the geometric mean of the singular values $\{\gamma_i\}$ of $\mathbf{HG}_\star$. Choose $\mathbf{V} = \mathbf{P}_h$ and transmit $\mathbf{x} = \mathbf{G}_\star\mathbf{P}_h\mathbf{d}$. Then

$$\mathbf{r} = \mathbf{Hx} + \mathbf{n} = \gamma\, \mathbf{Q}_h \mathbf{R}_h \mathbf{d} + \mathbf{n}. \tag{27}$$

Premultiplying by $\gamma^{-1}\mathbf{Q}_h^{\mathsf{H}}$ yields

$$\widetilde{\mathbf{r}} \triangleq \gamma^{-1}\mathbf{Q}_h^{\mathsf{H}}\mathbf{r} = \mathbf{R}_h\mathbf{d} + \widetilde{\mathbf{w}}_h, \tag{28}$$

where $\widetilde{\mathbf{w}}_h \triangleq \gamma^{-1}\mathbf{Q}_h^{\mathsf{H}}\mathbf{n}$ is white Gaussian noise with covariance $\mathsf{E}\big[\widetilde{\mathbf{w}}_h\widetilde{\mathbf{w}}_h^{\mathsf{H}}\big] = \frac{\sigma^2}{\gamma^2}\mathbf{I}_M$. By the harmonic–geometric mean inequality [31], it follows that

$$\mathsf{E}\big[\|\widetilde{\mathbf{w}}_h\|^2\big] \le \mathsf{E}\big[\|\mathbf{w}_h\|^2\big], \tag{29}$$

with equality iff $\gamma_1 = \cdots = \gamma_M$. The triangular system in (28) is decoded by backward SIC. Let $\rho_{\tau\nu}$ denote the (τ,ν) element of $\mathbf{R}_h$, so that $\rho_{\tau\tau} = 1$ and $\rho_{\tau\nu} = 0$ for $\tau > \nu$. The recursion is:

$$\hat{d}_M = \mathsf{DEC}_{\mathbb{A}}\{\tilde{r}_M\},$$
$$\hat{d}_\tau = \mathsf{DEC}_{\mathbb{A}}\left\{\tilde{r}_\tau - \sum_{\nu=\tau+1}^{M}\rho_{\tau\nu}\hat{d}_\nu\right\},\ \ \tau = M-1,\ldots,1.$$

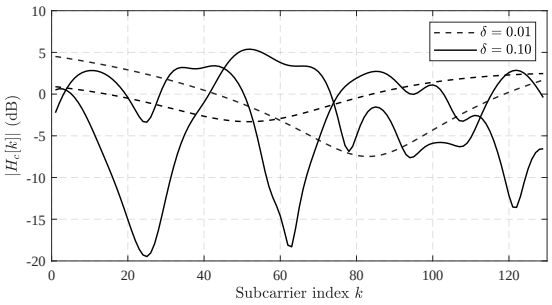

Fig. 1. Channel response $|H_c[k]|$ vs. subcarrier index $k \in \mathcal{K}$ for four Rayleigh block-fading realizations with $\delta \in \{0.01, 0.10\}$.

VI. Performance Evaluation

A. Simulation Setup

We evaluate CP–OFDM with rectangular pulse shaping ($h_{\mathrm{P}}[n] = 1$ for $0 \le n < L$, and 0 otherwise), IFFT size $N = 256$, CP length $l_g = 32$ ($L = N + l_g$), and sampling period T_s. The DAC interpolation filter is ideal lowpass: $|H_{\mathrm{I}}(f)| = 1$ for $|fT_s| \le \frac{1}{2}$ and 0 otherwise. A contiguous set of $K = 129$ subcarriers (index set $\mathcal{K}$) is activated symmetrically around the carrier frequency. OBR is penalized over the stopband $\mathcal{B} \triangleq \left\{f : \frac{1}{4T_s} + \frac{\Delta_f}{2} \le |f| \le \frac{1}{2T_s}\right\}$, with flat weight $W(f) = 1$ for $f \in \mathcal{B}$ and 0 otherwise. The channel is block-fading with exponential power delay profile (PDP) [32]:

$$h_c[n] = \mathrm{e}^{-\frac{n}{2\delta l_g}}\,\tilde{h}_c[n], \quad 0 \le n < l_g, \tag{30}$$

where $\{\tilde{h}_c[n]\}$ are i.i.d. circularly symmetric complex Gaussian random variables and $\delta > 0$ is a dimensionless delay-spread factor. Under (30), the exponential PDP has mean delay and RMS delay spread (in samples) both equal to $\delta\, l_g$. The per-subcarrier gains $H_c[k]$ are obtained via the N-point DFT of $\{h_c[n]\}$ and normalized *per realization* to fix the in-band energy: $\sum_{k\in\mathcal{K}}|H_c[k]|^2 = K$. Fig. 1 depicts typical realizations for $\delta \in \{0.01, 0.1\}$; larger δ yields stronger frequency selectivity across $\mathcal{K}$.

For each channel realization, we fix the transmit power budget to match PSP–OFDM, i.e., $P_{\max} = D$ so that $\mathrm{tr}(\mathbf{G}^{\mathsf{H}}\mathbf{G}) = D$. With $\mathbf{C}$, the reference MI $\mathcal{I}_0$ in (12) is computed via standard waterfilling over the top-D eigenmodes of $\mathbf{C}$ under the same power budget D. The design target is then set to $\mathcal{I}_{\min} = 0.99\,\mathcal{I}_0$ to ensure feasibility while keeping the operating rate arbitrarily close to the waterfilling bound at the same power. All schemes (proposed, PSP–OFDM [25]) are power-normalized to satisfy $\mathrm{tr}(\mathbf{G}^{\mathsf{H}}\mathbf{G}) = P_{\max}$ before evaluation.

B. Sidelobe Suppression Performance

Fig. 2 displays the ensemble-averaged PSDs attained by the proposed precoding strategies, namely, BSPM precoder $\mathbf{G}_\star$ and its CSIT-enhanced variants $\mathbf{G}_\star\mathbf{V}_h$ (ZF) and $\mathbf{G}_\star\mathbf{P}_h$ (SIC), under block-fading multipath channels with strong frequency selectivity ($\delta = 0.10$). Results are shown for redundancy

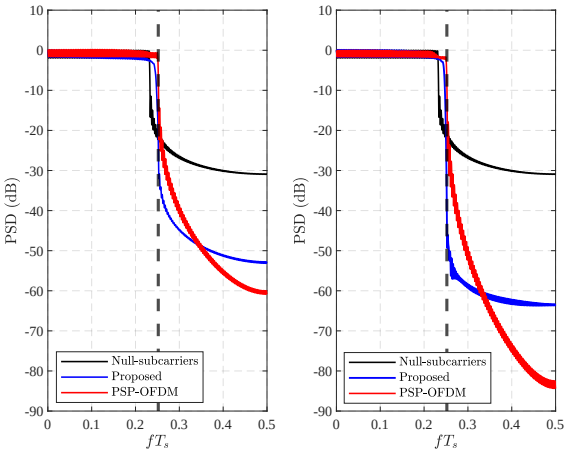

Fig. 2. PSDs of proposed BSPM precoder and PSP-OFDM precoders on a multipath block-fading channel with $N = 256$, $l_g = N/8$, $K = 129$ and $\delta = 0.10$; with (a) $R = 6$, and (b) $R = 10$.

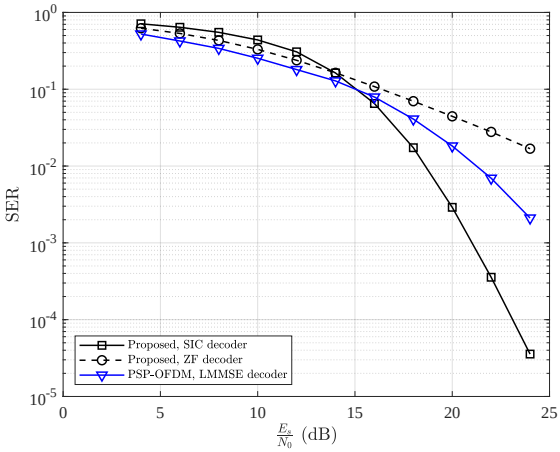

Fig. 3. SER performance of proposed BSPM precoder and PSP-OFDM precoders on a multipath block-fading channel for 16-QAM modulation (ZF and SIC), with $\delta = 0.10$ and $R = 6$.

values $R \in \{6, 10\}$. All three precoders share the same transmit covariance, and are therefore spectrally equivalent, yielding identical PSDs as per (4). For benchmarking, we include two alternative methods: (i) the PSP–OFDM scheme of [25], and (ii) a null-subcarrier baseline that zeroes out $R/2$ subcarriers at each band edge. Since both $\mathbf{G}_\star$ and the PSP–OFDM precoder are channel-dependent, the reported spectra are averaged over 1000 independent realizations of the random channel (30). For a fixed redundancy R, the BSPM-based designs exhibit significantly faster spectral decay near the occupied band, resulting in superior sidelobe suppression relative to PSP–OFDM. Quantitatively: For $R = 6$, the proposed precoders reduce the OBR by 15.64 dB, compared to 2.07 dB achieved by PSP–OFDM. For $R = 10$, the gap widens: 32.81 dB (proposed) versus 4.43 dB (PSP–OFDM). While PSP–OFDM achieves an asymptotic roll-off of f^{-2R-2}, its suppression is spread broadly. In contrast, BSPM focuses nulling power within the designated stopband $\mathcal{B}$; especially near the band edges, where leakage is most critical. This targeted shaping yields significantly stronger OBR reduction despite fewer suppressed modes.

C. Error rate performance

Symbol error rate (SER) results are averaged over 1000 independent realizations of the fading channel described in Section VI-A. A memoryless 16-QAM constellation is used, without forward-error correction. All detectors operate under perfect channel knowledge at the receiver. Fig. 3 shows that PSP-OFDM with LMMSE detection achieves the lowest SER at low SNR, whereas the proposed GMD-SIC receiver initially incurs error propagation. At moderate and high SNR, however, the triangular structure and semi-unitary front-end of GMD-SIC eliminate noise gain and interstream interference, producing the steepest SER decay and the best reliability.

The CSIT-aware ZF scheme based on SVD diagonalization remains above the SIC curve because its per-stream noise variance grows as σ^2/γ_i^2 on weak modes. In contrast, GMD-SIC equalizes the variance to σ^2/γ^2 before cancellation. In summary, while PSP-OFDM with LMMSE excels at low SNR, the proposed GMD–SIC receiver achieves the best performance at moderate-to-high SNR, establishing it as the most reliable scheme under favorable signal conditions.

VII. Conclusion

We presented a channel-aware spectral precoding framework for OFDM that minimizes OBR under power and MI constraints. The precoder is obtained via a fixed-point iteration and supports CSIT integration through spectrally-invariant unitary rotations. Simulation results confirm strong spectral confinement and improved error rates over prior designs. In particular, the proposed SIC receiver outperforms existing schemes at medium-to-high SNR, establishing it as a reliable solution for spectrally efficient, CSIT-aware transmission.

Appendix A
Solution to Problem (13)

Consider the SVD of $\mathbf{G} = \mathbf{U}\mathbf{\Sigma}\mathbf{V}^{\mathsf{H}}$, where $\mathbf{U} \in \mathbb{C}^{K\times D}$ is semi-unitary, $\mathbf{\Sigma} = \mathsf{Diag}\{\sigma_1, \ldots, \sigma_D\}$ with $\sigma_1 \geq \sigma_2 \geq \cdots \geq \sigma_D \geq 0$, and $\mathbf{V} \in \mathbb{C}^{D\times D}$ is unitary. Substituting in (13) yields

$$\min_{\mathbf{U},\mathbf{\Sigma}} \mathsf{Tr}\big(\mathbf{\Sigma}^2\big) \text{ s. to } \begin{cases} \log\left|\mathbf{I}_D + \mathbf{\Sigma}^2\mathbf{U}^{\mathsf{H}}\mathbf{C}\mathbf{U}\right| \geq \mathcal{I}_{\min}, & \text{(31a)} \\ \mathbf{U}^{\mathsf{H}}\mathbf{U} = \mathbf{I}_D. & \text{(31b)} \end{cases}$$

The problem is invariant to $\mathbf{V}$, and the objective does not depend on $\mathbf{U}$. Hence, for any fixed $\mathbf{\Sigma}$, the MI in (31a) is maximized by choosing $\mathbf{U}$ to span the top-D (principal) eigenspace of $\mathbf{C}$. Let $\lambda_1 \geq \lambda_2 \geq \cdots \geq \lambda_K \geq 0$ denote the ordered eigenvalues of $\mathbf{C}$. Then the problem reduces to

$$\min_{\sigma_1^2,\ldots,\sigma_D^2} \sum_{l=1}^{D} \sigma_l^2 \quad \text{s.to} \begin{cases} \sum_{l=1}^{D} \log\left(1 + \lambda_l\sigma_l^2\right) \geq \mathcal{I}_{\min}, & \text{(32a)} \\ \sigma_1^2 \geq \sigma_2^2 \geq \cdots \geq \sigma_D^2 \geq 0. & \text{(32b)} \end{cases}$$

If $\lambda_l = 0$ for some i, the corresponding term contributes zero MI and is set inactive; the active set size q satisfies

$q \leq \min\{D, \text{rank}(\mathbf{C})\}$. Problem (32) is convex, and its KKT conditions yield the reverse waterfilling solution

$$\sigma_l^2 = \left[\gamma - \frac{1}{\lambda_l}\right]^+, \qquad l = 1, \ldots, D, \tag{33}$$

where $[x]^+ \triangleq \max\{x, 0\}$, and $\gamma > 0$ is chosen to satisfy

$$\sum_{l=1}^{D} \log\left(1 + \lambda_l \left[\gamma - \frac{1}{\lambda_l}\right]^+\right) = \mathcal{I}_{\min}. \tag{34}$$

Equivalently,

$$\sum_{l=1}^{D} [\log\gamma + \log\lambda_l]^+ = \mathcal{I}_{\min}, \tag{35}$$

which determines γ efficiently. Since q is the number of active modes (for which $\gamma > 1/\lambda_l$), then

$$\sum_{l=1}^{q} (\log\gamma + \log\lambda_l) = \mathcal{I}_{\min} \Rightarrow \log\gamma = \frac{1}{q}\left(\mathcal{I}_{\min} - \sum_{l=1}^{q} \log\lambda_l\right) \tag{36}$$

Define the thresholds $J_0 \triangleq 0$, $J_{l'} \triangleq \log \dfrac{\lambda_1\lambda_2\cdots\lambda_{l'}}{\lambda_{l'+1}^{l'}}$ for $l' = 1, \ldots, D-1$, and $J_D \triangleq +\infty$, which satisfy $J_0 \leq J_1 \leq \cdots \leq J_D$. Then q is the unique index such that $J_{q-1} \leq \mathcal{I}_{\min} < J_q$. At the optimum, the minimum required power is

$$P_0 = \sum_{l=1}^{D} \sigma_l^2 = \left(\frac{e^{\mathcal{I}_{\min}/q}}{\mathcal{G}_q} - \frac{1}{\mathcal{H}_q}\right) q, \tag{37}$$

where $\mathcal{G}_q \triangleq \left(\prod_{l=1}^{q} \lambda_l\right)^{1/q}$ and $\mathcal{H}_q \triangleq \dfrac{q}{\sum_{l=1}^{q} \lambda_l^{-1}}$ are respectively the geometric and harmonic means of $\{\lambda_1, \ldots, \lambda_q\}$.

REFERENCES

[1] A. A. Zaidi, R. Baldemair, H. Tullberg, H. Bjorkegren, L. Sundstrom, J. Medbo, C. Kilinc, and I. Da Silva, "Waveform and numerology to support 5G services and requirements," *IEEE Commun. Mag.*, vol. 54, no. 11, pp. 90–98, 2016.

[2] B. Farhang-Boroujeny, "OFDM versus filter bank multicarrier," *IEEE Signal Process. Mag.*, vol. 28, no. 3, pp. 92–112, 2011.

[3] L. Wei and C. Schlegel, "Synchronization requirements for multi-user OFDM on satellite mobile and two-path rayleigh fading channels," *IEEE Trans. Commun.*, vol. 43, no. 2/3/4, pp. 887–895, 1995.

[4] M. Sharique and A. K. Chaturvedi, "A new family of time-limited nyquist pulses for OFDM systems," *IEEE Commun. Lett.*, vol. 20, no. 10, pp. 1943–1946, 2016.

[5] M. Faulkner, "The effect of filtering on the performance of OFDM systems," *IEEE Trans. Veh. Technol.*, vol. 49, no. 5, pp. 1877–1884, 2000.

[6] J. Park, E. Lee, S.-H. Park, S. Raymond, S. Pyo, and H.-S. Jo, "Modeling and analysis on radio interference of OFDM waveforms for coexistence study," *IEEE Access*, vol. 7, pp. 35132–35147, 2019.

[7] T. Frank, A. Klein, and T. Haustein, "A survey on the envelope fluctuations of DFT precoded OFDMA signals," in *in Proc. IEEE Int. Conf. Commun.,*, 2008, pp. 3495–3500.

[8] T. Weiss, J. Hillenbrand, A. Krohn, and F.K. Jondral, "Mutual interference in OFDM-based spectrum pooling systems," in *in Proc. IEEE Veh. Technol.*, 2004, vol. 4, pp. 1873–1877 Vol.4.

[9] L. Díez, J. A. Cortés, F. J. Cañete, E. Martos-Naya, and S. Iranzo, "A generalized spectral shaping method for OFDM signals," *IEEE Trans. Commun.*, vol. 67, no. 5, pp. 3540–3551, 2019.

[10] E.l Güvenkaya, A. Şahin, E. Bala, R. Yang, and H. Arslan, "A windowing technique for optimal time-frequency concentration and aci rejection in OFDM-based systems," *IEEE Trans. Commun.*, vol. 63, no. 12, pp. 4977–4989, 2015.

[11] M. M. Naghsh, E. Haj Mirza Alian, S. Khobahi, and O. Rezaei, "A majorization–minimization approach for reducing out-of-band radiations in OFDM systems," *IEEE Commun. Lett.*, vol. 21, no. 8, pp. 1739–1742, 2017.

[12] A. Tom, A. Şahin, and H. Arslan, "Suppressing alignment: Joint PAPR and out-of-band power leakage reduction for OFDM-based systems," *IEEE Trans. Commun.*, vol. 64, no. 3, pp. 1100–1109, 2016.

[13] S. Pagadarai, R. Rajbanshi, A. M. Wyglinski, and G. J. Minden, "Sidelobe suppression for OFDM-based cognitive radios using constellation expansion," in *IEEE Wireless Commun. Netw. Conf. (WCNC)*, 2008, pp. 888–893.

[14] S. Brandes, I. Cosovic, and M. Schnell, "Reduction of out-of-band radiation in OFDM systems by insertion of cancellation carriers," *IEEE Commun. Lett.*, vol. 10, no. 6, pp. 420–422, 2006.

[15] J. F. Schmidt, D. Romero, and R. López-Valcarce, "Active interference cancellation for OFDM spectrum sculpting: Linear processing is optimal," *IEEE Commun. Lett.*, vol. 18, no. 9, pp. 1543–1546, 2014.

[16] J. van de Beek, "Orthogonal multiplexing in a subspace of frequency well-localized signals," *IEEE Commun. Lett.*, vol. 14, no. 10, pp. 882–884, 2010.

[17] J. van de Beek and F. Berggren, "N-continuous OFDM," *IEEE Commun. Lett.*, vol. 13, no. 1, pp. 1–3, 2009.

[18] L. Dan, C. Zhang, J. Yuan, P. Wen, and B. Fu, "Improved N-continuous OFDM using adaptive power allocation," in *" in Proc. IEEE 8th Annu. Comput. Commun. Workshop Conf.*, 2018, pp. 937–940.

[19] C.-D. Chung and K.-W. Chen, "Spectrally precoded OFDM without guard insertion," *IEEE Trans. Veh. Technol.*, vol. 66, no. 1, pp. 107–121, 2017.

[20] M. Mohamad, R. Nilsson, and J. Van De Beek, "A novel transmitter architecture for spectrally-precoded OFDM," *IEEE Trans. Circuits Syst. I*, vol. 65, no. 8, pp. 2592–2605, 2018.

[21] R. Kumar, K. Hussain, and R. López-Valcarce, "Mask-compliant orthogonal precoding for spectrally efficient OFDM," *IEEE Trans. Commun.*, vol. 69, no. 3, pp. 1990–2001, 2021.

[22] K. Hussain, R. López-Valcarce, F. Rey, J. Sala-Alvarez, and J. Villares, "Sidelobe suppression for multicarrier signals via structured spectral precoding," *IEEE Trans. Commun.*, pp. 1–1, 2024.

[23] H.-M. Chen, W.-C. Chen, and C.-D. Chung, "Spectrally precoded OFDM and OFDMA with cyclic prefix and unconstrained guard ratios," *IEEE Trans. Wireless Commun.*, vol. 10, no. 5, pp. 1416–1427, 2011.

[24] M. Ma, X. Huang, B. Jiao, and Y. J. Guo, "Optimal orthogonal precoding for power leakage suppression in DFT-based systems," *IEEE Commun. Lett.*, vol. 59, no. 3, pp. 844–853, 2011.

[25] W.-C. Chen, C.-D. Chung, and P.-H. Wang, "Pre-equalized and spectrally precoded OFDM," *IEEE Trans. Veh. Technol.*, vol. 71, no. 7, pp. 7472–7486, 2022.

[26] R. López-Valcarce, "General form of the power spectral density of multicarrier signals," *IEEE Trans. Commun.*, vol. 26, no. 8, pp. 1755–1759, 2022.

[27] S.P. Boyd and L. Vandenberghe, *Convex Optimization*, Cambridge Univ. Press, Cambridge, U.K., 2004.

[28] J.R. Magnus and H. Neudecker, *Matrix Differential Calculus With Applications in Statistics and Econometrics*, John Wiley, New York, 2019.

[29] I. V. L. Clarkson, "Orthogonal precoding for sidelobe suppression in DFT-based systems using block reflectors," in *Proc. IEEE Int. Conf. Acoust., Speech, Signal Process.*, 2017, pp. 3709–3713.

[30] Yi J., William W. H., and Jian L., "The geometric mean decomposition," *Linear Algebra Appl.*, vol. 396, pp. 373–384, 2005.

[31] G. H. Hardy, J. E. Littlewood, and G. Pólya, *Inequalities*, Cambridge University Press, Cambridge, UK, 2nd edition, 1952.

[32] H. Arslan and T. Yucek, "Delay spread estimation for wireless communication systems," in *Proc. IEEE 8th Symp. Comput. and Commun.*, 2003, pp. 282–287.